On the Mechanisms of DC Conduction in Electrospun PLZT/PVDF Nanocomposite Membranes

James C. Sampson[1], Ashok Batra[1], Matthew E. Edwards[1], Ashok Vaseashta[2,3*], Chris R. Bowen[4], and Sushma Kotru[5]

[1]Department of Physics, Chemistry, and Mathematics, College of Engineering, Technology and Physical Sciences, Alabama A&M University, Normal (Huntsville), AL 35762 USA
[2]International Clean Water Institute, Manassas, VA 20112, USA
[3]Biomedical Engineering and Nanotechnologies Institute, Riga Technical University, Riga, LV, Latvia
[4]Department of Mechanical Engineering, University of Bath, Bath, UK
[5]Department of Electrical and Computer engineering, Center for Materials for Information Technology, University of Alabama, Tuscaloosa, AL 35487 USA

*Corresponding author: prof.vaseashta@ieee.org

Abstract: Designing dielectric nanocomposite films with excellent dielectric properties is of strategic importance for a variety of applications requiring pressure sensing, energy harvesting and storing, and biomedical technology. Hence, the present investigation aims at studying the dielectric properties of lead lanthanum zirconate titanate (PLZT)/poly(vinylidene fluoride) (PVDF) nanocomposite based membranes fabricated using traditional electrospinning techniques. The composites were investigated for structural and electrical conductivity properties at varying temperatures. While the Scanning Electron microscope revealed beaded and unannealed micro/nanofibers, the observations of temperature-dependent electrical conductivity imply that the charge carrier transport phenomena involve more than one conduction mechanism. This is an interesting observation and can be explained in terms of the contents and porosity of the composites. As compared to PVDF, PLZT/PVDF nanocomposite films have somewhat better conductivity. The space charge limited current (SCLC) was the dominant mechanism at high voltages, while the Schottky–Richardson conduction mechanism was dominating at high temperature, according to observed J–V characteristics. The DC activation energy was found to be different, as expected, due to the dynamically heterogeneous nature of PLZT aggregates within the polymer matrix; however, the films exhibit the well-known Arrhenius relationship. This indicates that the dominant conduction mechanism is observed to be electronic and thermally activated.

Keywords*:* electrospinning, membrane, nanofiber, PVDF, PLZT

1. Introduction

Poly(vinylidene fluoride) (PVDF), also known as poly(1,1-difluoroethylene), is a high-performance polymer and has useful electroactive features such as piezoelectricity, pyroelectricity, ferroelectricity, and optoelectronics. PVDF is made up of around 50% lamellar crystals with a thickness of tens of nanometers and a length of up to 100 nanometers embedded in an amorphous matrix. PVDF and its copolymers exhibit a low density (1.78 g/cm^3) when compared to other fluoropolymers like polytetrafluoroethylene; as a result, PVDF and its copolymers are attractive materials for the additional number of possible organic microelectronics applications, such as electro-optic transducers, waveguides, sensors, actuators, energy harvesting, and electro-optic transducers memory, and biomimetic robotics [1-6].

PVDF, often referred to by its trade name Kynar®, is a high purity engineering thermoplastic and highly polar material. As per the International Association of Plastics Distribution (IPPD), PVDF is a semi-crystalline, high purity thermoplastic fluoropolymer, where electrical characteristics are caused by the polarized structure between hydrogen (δ+) and fluorine (δ−). The repeat unit of $(–CH_2–CF_2–)_n$ or $(CH_2\text{-}CF_2)_n$, where the carbon-hydrogen bonds with the electrically polar carbon-fluorine, can take up to several stable configurations. The crystalline structures of PVDF may be present in at least four types: α, β, γ, and δ phases. PVDF β phase (form I) is an all-trans planar zigzag conformation (TTTT), PVDF α phase (form II) is a trans-gauche twist conformation (TGTG′), PVDF δ phase (form IV) is a different packing structure of PVDF α phase, and PVDF γ phase (form III) is an intermediate conformation of PVDF β and α phases (TTTGTTTG′). In the case of β and γ phases, all dipoles of individual molecules are arranged parallel to each other producing a non-zero dipole moment, and hence they induce polarity. Since the electroactive properties of a material depend on its polar structure, the β phase of PVDF shows the highest electroactive properties due to the highest dipole moment (8×10^{-30} C.m). Two forms β (or I) and α (or II) phases are of particular importance. The α phase can be converted into the β form by stretching and electrically poling with an appropriate electric field. All-trans configurations in the β form exist in the molecular groups, with molecules assembled to provide a polar unit cell.

Several research investigations have highlighted the benefits of using nanoparticles, including carbon nanotubes dispersed in a polymer matrix to design and fabricate multifunctional materials with improved strength [7-9], including improvement in certain electrical properties [10]. Piezoelectric sensors have a high sensitivity and stability, but they are unable to sense static pressures since the surface charge decays under static loads, limiting their usage as pressure sensors. Many piezoelectric materials are ceramic-based and rigidity, brittleness, toxicity, high density, lower voltage coefficient, and lack of

design flexibility are some of the shortcomings of traditional piezoelectric materials. The design parameters, such as flexibility, application frequency, and available volume, limit the choice of certain piezoelectric materials for a specific energy-based application. The high contact resistance between conductive materials may also critically restrict the application of the sensors. Piezoelectric polymers, such as PVDF, are therefore of interest as they satisfy most of the abovementioned criteria, in addition to high stability, low power consumption, and simple construction. Ferroelectric smart materials have been utilized for several applications because their notably large piezoelectric coefficients, high pyroelectric coefficients, electro-optic properties, and dielectric susceptibilities exist [1]. They are used as high energy density capacitors, sensors, actuators, ultrasonic imaging, pyroelectric thermal imaging, electro-optic light valves, gate insulators in transistors, multiferroic transducers, thin-film memory elements, and energy harvesters. As an example, lead zirconate (lanthanum) titanate (PLZT) is a ferroelectric material that manifests both pyroelectric and piezoelectric characteristics upon polarization [2]. These achievements in the area of sensor technology were obtained because its high piezoelectric coefficients, electromechanical coupling coefficients, and dielectric constants manifest. To combine the attractive properties of PLZT and PVDF, composite materials are being considered.

The probable dc conduction mechanism(s) and nature of charge transport in PLZT/PVDF nanocomposite are therefore investigated in this paper since conduction mechanisms are not restricted to classical conduction and transport methods. This investigation may aid in the application of this material as it improves our knowledge of the material for future studies. Composites in the form of fiber membranes are gaining interest as a result of their potential in large-area low-voltage devices. The 0–3 connectivity composite, which consists of a three-dimensionally connected polymer matrix filled with isolated active ferroelectric ceramic particles, is the most basic of the composites studied. One of the most attractive features of the 0–3 design is its versatility in the fabrication of a variety of geometric forms, including thin/thick films and certain molded shapes. In this work, we have investigated the probable conduction mechanisms in PLZT nanocomposite films. In the light of some known conduction mechanism(s) models like Schottky emission, tunneling, space charge limited conduction (SCLC), intrinsic conduction, Poole–Frenkel (PF) conduction processes [11-15], an analysis is investigated here to explain conduction mechanism(s) in nanocomposite membranes fabricated by electrospinning.

2. Experimental details

2.1. Nanomiser® Technique for Nanoparticles Fabrication

The nanoparticles modified PZT (named MPLZT) were procured and prepared by a propriety method to produce a variety of high purity ceramics, mixed metal oxide, and metal nanopowder using the nanospray process by Micro-coating Inc., Georgia, USA. In this process, a proprietary Nanomiser®the device is used to produce large quantities of aerosols with controllable, narrow droplet size distributions. The micrograph shows some agglomeration of particles Figure 1. The particles are of the order less than 30 nm with equal size.

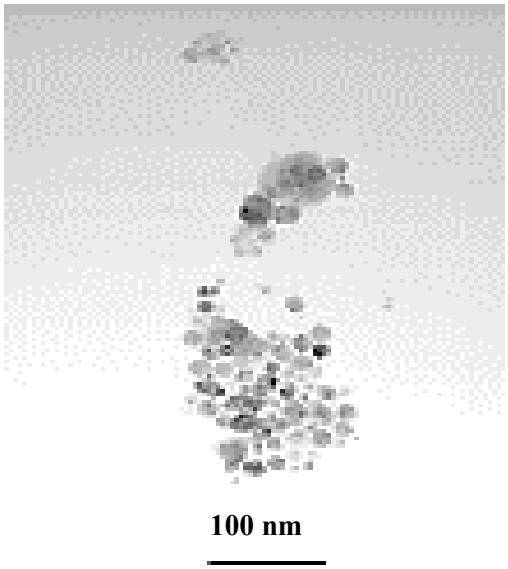

Figure 1 A transmission electron micrograph (TEM) of nanoparticles of MPLZT ($Pb_{0.93}La_{0.07}Zr_{0.3}Ti_{0.7}O_3$)

2.2. Electrospun Membrane Fabrication

The electrospinning process is based on an electro-hydrodynamic phenomenon in which the fibers are made from polymer solutions or molten polymers [16,17]. The surface and inner morphology of the resultant nanofibers can be changed by the process variables such as the polymer type and concentration, the type of a solvent, the needle to the collector distance, the flow rate, the applied electric field, the temperature, and humidity [18]. Since the properties of electrospun nanofibers are significantly affected by the fabrication parameters, a PVDF powder (MW 534000, Sigma-Aldrich) was dissolved in the solution of dimethylformamide (analytical standard, Fisher Scientific) to yield a polymer solution with a concentration of 20 wt. %. The solution was mechanically stirred for 3 h at a constant speed of 100 rpm

on a hot plate set at 60 °C. Electrospinning of the PVDF solution was carried out with an Inovenso laboratory-scale electrospinning apparatus. A constant voltage of 20 kV with the negative polarity was applied to the stainless needle of 18 gauge located 18 cm from the grounded collector plate. The flow rate of the solution for all samples was set at 6 mL/hr^{-1}, and the time of electrospinning was approximately 60 min. The ambient temperature during electrospinning was approximately 25° C, and the ambient humidity was ~ 60%. The nanofibers produced by this method were collected on aluminum foil and DC studies were conducted using electrospun fibers membranes by removing them from the aluminum foil – by cutting to an appropriate size and applying a copper tape with a conducting adhesive on both sides of the PVDF membrane to form a full-face electrode capacitor. It is worth mentioning that electrospun nanofibers exhibit many exceptional properties such as a large surface area, high aspect ratio, flexible surface, superior mechanical properties, and tunable surface morphologies [19]. The fibers also provide a very large surface area per unit mass. As a result, only a small amount of material is required, and there is very little waste. Another uniquely important advantage is that nanofibers prepared through a simple and scalable electrospinning process can eliminate the need for conventional direct-contact corona poling in ferroelectric materials, as was used in our experimentation. The composition of PVDF-nanocomposite solution is described in table 1, including sample nomenclature.

Table 1: Composition of PVDF solution, DMF = Dimethylformamide, MEK = Methyl Ethyl Ketone, and SWCNT = single-walled carbon nanotubes.

PVDF (grams)	DMF/MEK (mL)	PLZT (grams)	Sample code
2.0	30	0.00	PVDF
2.0	30	0.045	MPLZT-1
2.0	30	0.074	MPLZT-2
2.0	30	0.114	MPLZT-3
2.0	30	0.212 +SWCNT	MPLZT-4

2.3. DC Conductivity Measurements

To eliminate extrinsic charge carriers the samples were short-circuited and annealed at 50° C for 2 h after the fabrication procedure. The approximate thickness of the composite films was 0.24 mm and the bulk

DC conductivity wase obtained using Ohm's law as per the Drude model:

$$\sigma_{dc} = I.t / V.A \quad (1)$$

where I is the current in amperes and V is the applied voltage in volts over the samples. The parameters A and t are the area and thickness of the composite membrane, respectively. Two terminal electrical measurements were performed for DC measurement, utilizing a Keithley model 6517.

2.4. Surface Microstructures

The surface morphology of the electrospun PVDF nanofiber mat was analyzed using a scanning electron microscope) for JOEL, USA. The fibers were coated with a thin film of gold before observation using scanning electron microscopy (SEM) at an accelerating voltage of 2 kV at typically 5000X magnification. Figure 2 below shows a typical SEM image of the electrospun PVDF nanofiber mat. The fibers are randomly oriented forming a web of nanofibers, with only a few beads formed during electrospinning. An inset shows a section of aligned fibers ~ 100 nm forming a mesh within the composite of PVDF and MPLZ.

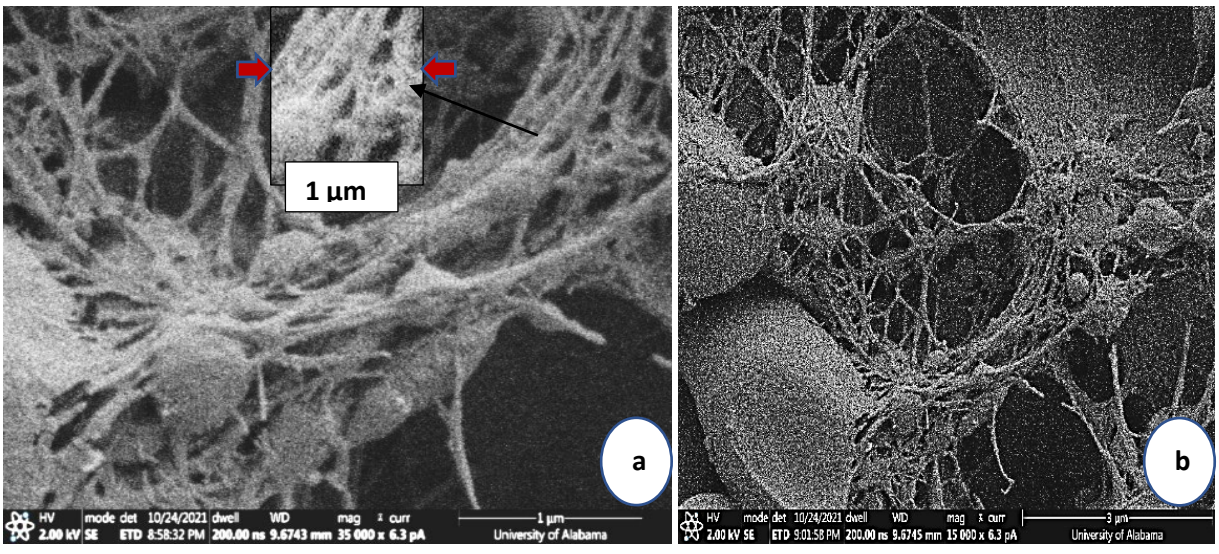

Figure 2 Scanning electron micrographs of electrospun nanocomposite membranes (a) PVDF (b) MPLZT-4.

3. Results and Discussion

Among the conduction mechanisms being investigated in this investigation, some depend on the electrical properties at the electrode-dielectric contact. These conduction mechanisms are called

injection-limited or electrode-limited conduction mechanisms. Other conduction mechanisms depend on the properties of the dielectric itself and are called transport-limited or bulk-limited conduction mechanisms. Since several conduction mechanisms may all contribute to the conduction current through the dielectric film at the same time, it is necessary to distinguish among these conduction mechanisms. Furthermore, several conduction mechanisms depend on the temperature, and thus measuring the temperature-dependent conduction currents may provide a way to know the constitution of the conduction currents.

The electrode-limited conduction mechanisms include (1) Schottky or thermionic emission, (2) Fowler-Nordheim tunneling, (3) direct tunneling, and (4) thermionic-field emission. The bulk-limited conduction mechanisms include (1) Poole-Frenkel emission, (2) hopping conduction, (3) ohmic conduction, (4) space-charge-limited conduction, (5) ionic conduction, and (6) grain-boundary-limited conduction, as shown in figure 3 below.

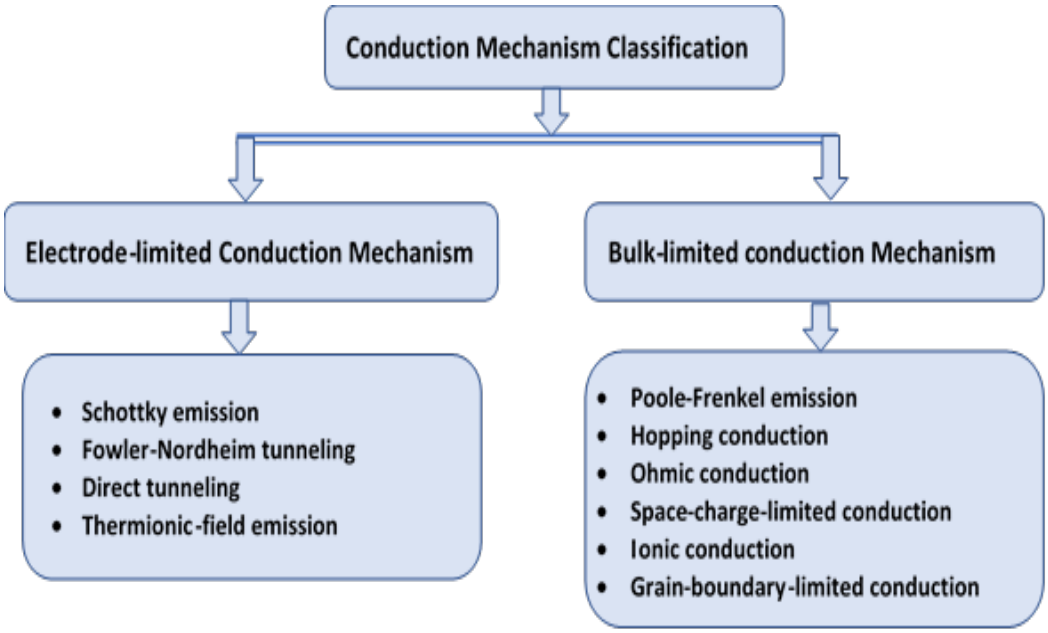

Figure 3: Classification of conduction mechanisms in dielectric films

3.1. Steady-state Electrical Conduction

When the influence of absorption current reduces the steady-state conduction current or the leakage current is reasonably constant over time [20], the steady-state conductivity can be observed. Leakage currents are generally measured after a period of testing at the device held at a certain test temperature. The currents were recorded after 5 seconds at the stabilized test temperature of the sample and the applied

electric field. Figure 4 shows the current density-voltage (J–V) characteristics of the membranes at 50°C in a voltage range of 1–20 V, which shows an increase in current density with the applied voltage. From the linear behavior with a positive slope, one can simply deduce the ohmic conduction mechanism applicable to both composite films with the power law of the form, viz., $J \alpha V^n$, where n is the power index. The mode of electric transport is governed by the resistance of the membrane samples and directed by thermally activated charge carriers in the ohmic conduction region.

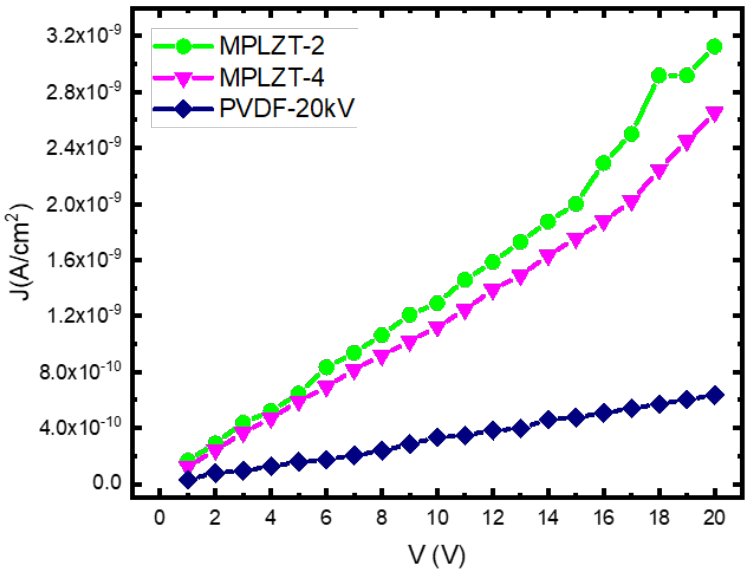

Figure 4. J-V Characteristics of MPLZT-2 and MPLZT-4 and PVDF-20kV electrospun films.

It is observed from the J–V curve that the current in MPLZT-2 composite film is higher than the pure PVDF nanofiber membrane. This can be explained by incorporating PLZT in the PVDF solution, which may be forming charge transfer interfaces. However, in the case of MPLZT-4 film with a higher particle content, the current is lower due to the presence of the conductive MWCNT in the solution. Since in these samples, dipolar polarization does exist, the role of dipolar and space charge polarization contribution to conduction mechanisms cannot be ruled out, in structurally heterogeneous composite membranes. Therefore, the results obtained in this investigation were examined in the framework of other potentially relevant types of conduction mechanism(s) present due to the complex nature of charge transport [21]. Other relevant and possible conduction processes include SCLC [22], Schottky [23], and PF [24] mechanisms. It is worth mentioning that the membranes consist of nanofibers with PLZT of ~ 30 nm size and hence demonstrate slightly higher conductivity as compared with PVDF. In general, modeling of thermal conductivity of composites, by modifying both the thermal conductivity of the

matrix and particles to take into account the strong scattering of the energy carriers with the surface of the nanoparticles, it is observed that the particle size effect shows up on the thermal conductivity of nanocomposites through the collision of the particles. The thermal conductivity of composites with metallic particles depends strongly on the relative size of the particles concerning the intrinsic coupling length, and the ratio between the electron and phonon thermal conductivities. The size dependence of the composite thermal conductivity appears not only through the interfacial thermal resistance but also by utilizing the electron-phonon coupling. Furthermore, at the non-diluted limit, the interaction among the particles is taken into account through a crowding factor, which is determined by the effective volume of the particles. Also, since surface conduction can contribute to the total conduction process, conductivity will increase with the incorporation of nanoparticles.

3.2. Space-charge limited conduction (SCLC)

In the SCLC regime, the current is dominated by charge carriers injected from the contacts and the current-voltage characteristics become quadratic ($I \sim V^2$). The current is then only dependent on the mobility and no more on the charge carrier density, hence, the mobility can be estimated from a simple current-voltage measurement. This is in contrast to Ohmic conduction, where the current is mainly driven by the mobile charge carriers being intrinsically present in a material so that the charge carrier density needs to be known to determine the mobility. For the current study, the charge is injected at the electrode–polymer interface that has a large excess charge carrier density at the injecting electrode, leading to the SCLC current flow. The space charge limited current density is represented by:

$$J = \frac{9}{8} \varepsilon \mu \frac{V^2}{d^3} \tag{2}$$

where J is the current density of SCLC at voltage V and d is the thickness of samples. The parameters ε and μ are permittivity and permeability of the material, respectively.

From Eq. (2) it is evident that J is inversely proportional to d^3. The large negative value of slope with linear nature of the characteristics is governed by the SCLC mechanism [22]. The linear relationship that exists at higher voltages of J versus V^2 in the PVDF film (Fig. 5) indicates the existence and predominance of the SCLC mechanism. However, it can be observed that the non-linear nature of J–V^2 curve illustrates the absence of the SCLC conduction mechanism in nanocomposite films (membranes).

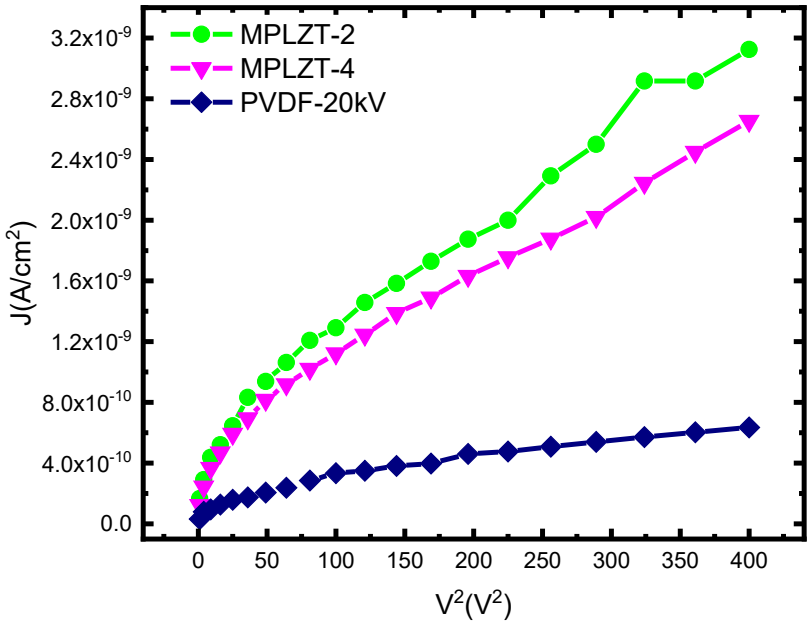

Figure 5. Variation of current density (J) with square of applied voltage (V^2) for MPLZT-2 and MPLZT-4 and PVDF-20kV electrospun films.

3.3. Tunneling or Fowler–Nordheim Mechanism

The electrode-limited conduction mechanisms depend on the electrical properties at the electrode-dielectric contact. The quantum mechanism predicts that the electron wave function will penetrate through the potential barrier when the barrier is thin enough (<100 ˚A). Hence, the probability of electrons existing at the other side of the potential barrier is not zero because of the tunneling effect. Fowler-Nordheim (F-N) tunneling occurs when the applied electric field is large enough so that the electron wave function may penetrate through the potential barrier into the conduction band of the dielectric [25, 26]. Hence, the current is produced without the transport of charge carriers in the conduction band or the valance band. The Fowler–Nordheim relation for J can be expressed as:

$$log\frac{J}{V^2} = logA - \frac{\varphi}{V} \quad (3)$$

where A = $\frac{q^3}{8\pi h\varphi_B}$, and $\varphi = \frac{8\pi\sqrt{(2qm^8}}{3}\frac{)}{h}\ \varphi^{3/2}$

J, V, q, m, φ_B* are the current density, applied voltage, electronic charge, tunneling effective mass, and barrier potential, respectively. If the tunneling effect prevails, then a log of J/V^2 versus 1/V

plot (Fig. 6) should exhibit a linear nature with a negative slope. For the study under investigation, the samples are of thickness approximate 0.15mm which is relatively thicker; therefore, one can exclude the tunneling effect. It is observed that plots have neither linear characteristic nor negative slope, thereby indicating the absence of tunneling effect in films investigated.

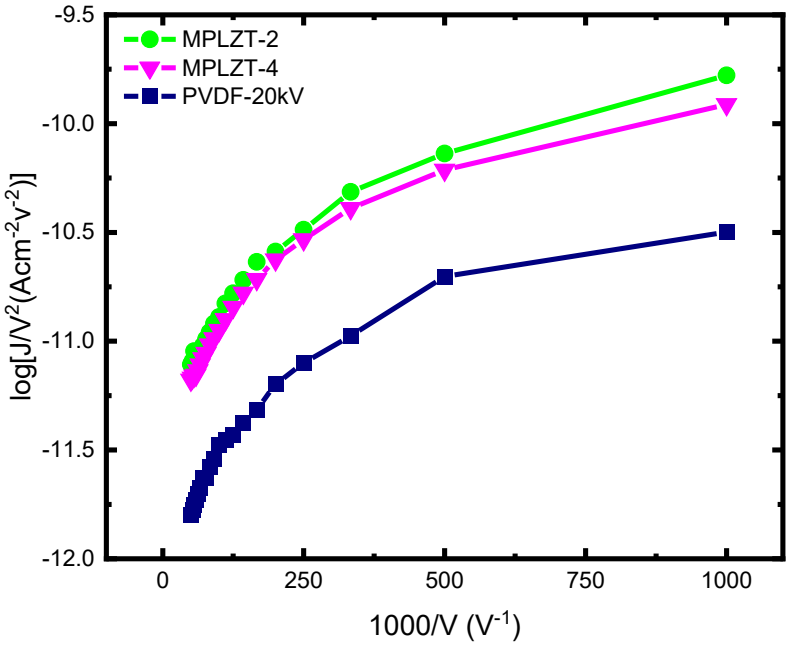

Figure 6. Fowler-Nordheim plots of MPLZT-2 and MPLZT-4 and PVDF-20kV electrospun films at 50°C.

3.4. Poole–Frenkel (PF) conduction

The process of Poole–Frenkel (PF) conduction is similar to that of well-known Schottky thermal emission and occurs due to the trapped electrons or holes being excited by heat [27,28]. Bulk-limited electric transport arises as a result of electron emission from trapping centers in samples under test, due to the effects of temperature and electric field. Hence, field-assisted thermal ionization is another term for PF conduction. The conductivity of the PF field is stated as:

$$log\sigma = log\sigma_0 + \frac{\beta_{PF}}{2kT}\sqrt{F} \quad (4)$$

where *F*, k, T are the Poole-Frenkel coefficient under static electric field, Boltzmann constant, and absolute temperature, respectively. The linearity of log σ versus $F^{1/2}$ or log σ versus $V^{1/2}$ plots with a positive slope indicates the presence of the PF mechanism. From Figure 7 it can be seen that the plot for both the films exhibits a nonlinearity without any particular slope character (positive or negative); ruling

out the possibility of PF conduction mechanism in the films under investigation. It is worth assuming, that it may be due to the presence of space charges accumulated near the electrodes creating non-uniform electric field distribution between the electrodes.

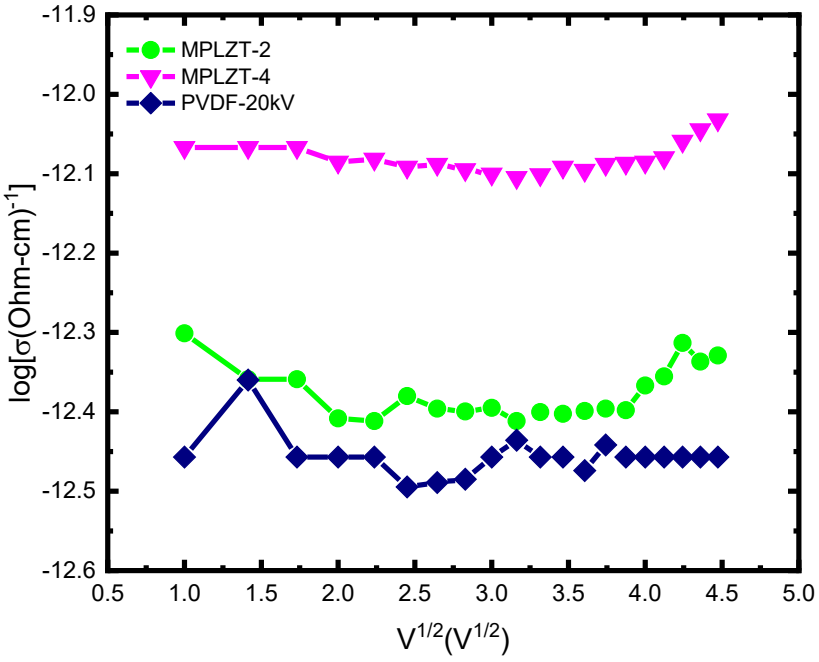

Figure 7. PF (PF) of MPLZT-2 and MPLZT-4 and PVDF-20kV electrospun films at 50°C.

3.5. Schottky–Richardson mechanism

An electric field at a metal-polymer interface interacts with the image force and lowers the potential barrier in the Schottky-type conduction mechanism. For the Schottky–Richardson, the model current-voltage relationship is expressed as,

$$logJ = logAT^2 - \frac{\varphi}{kT} + \beta_s F^{1/2} \quad (5)$$

where, $\beta_S = \frac{q\sqrt{\frac{q}{4\pi\varepsilon_r\varepsilon_0}}}{kT}$, F, A, T, $\varphi, k, q, \varepsilon_r,$ ε_0 are electric field, effective Richardson constant, absolute temperature, Schottky barrier height, Boltzmann constant, electronic charge, optical dielectric constant, and permittivity in a vacuum, respectively [29,30].

The linear slope of the J–$V^{1/2}$ curve with a positive slope governs the Schottky–Richardson process. The curves in Figure 8 are nonlinear, albeit showing a positive slope, especially at higher voltages. The most likely source of the divergence is the accumulation of space charges near the electrodes, resulting in non-uniform field distribution between the electrodes.

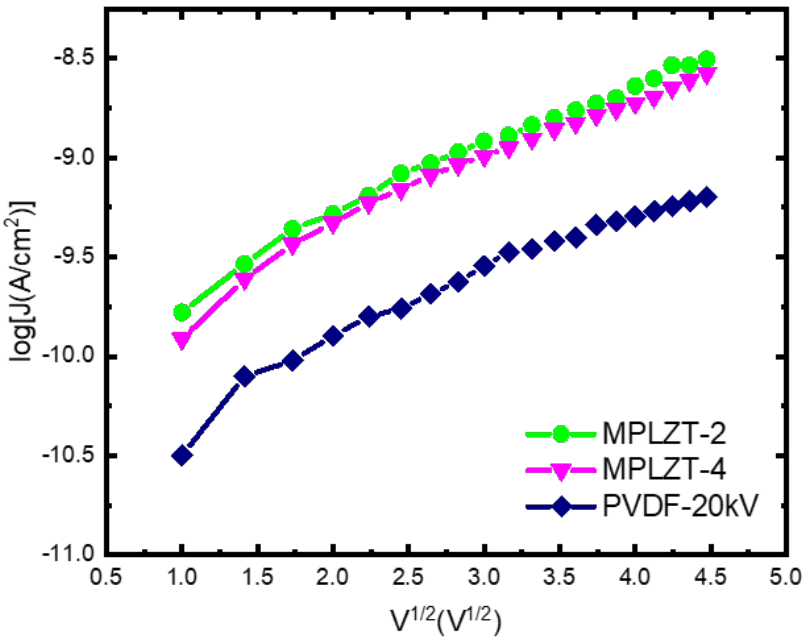

Figure 8. Schottky plots of MPLZT-2 and MPLZT-4 and PVDF-20kV electrospun films at 50°C.

Furthermore, the linear nature of the curve at higher voltages indicates electronic-type conduction that may be caused by either the Schottky emission mechanism or the Poole-Frenkel mechanism [31, 32]. In the plot of log (J/T^2) versus 1000/T, the Richardson line shows linearity with a negative slope, (Fig. 9). The negative slope in both composites films specifies the relevance of the Schottky–Richardson mechanism. Furthermore, it can be observed that the current density is strongly dependent on temperature; see (Fig.10), where it is observed that linear increment of log J exists with elevated temperature and sharp linearity persists in higher temperature regions. This behavior is an indication of the absence of any thermodynamic transition in the chosen temperature range. The strong temperature dependency follows Schottky–Richardson conduction mechanism [31,32].

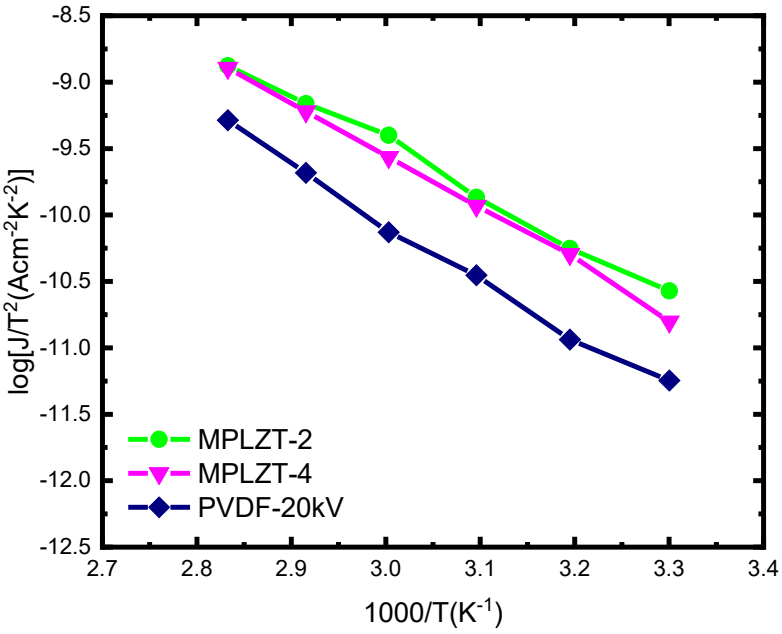

Figure 9. Richardson plots of MPLZT-2 and MPLZT-4 and PVDF-20kV at the applied voltage of 10V.

3.6. DC–Electrical Conductivity

The graph between electrical conductivity and temperature was plotted to elucidate the effect of PLZT on the dc conductivity of the PVDF nanocomposite membrane. The temperature dependence of dc conductivity in the temperature range of 20–80°C for samples is shown in Figure 11. It is observed that the dc conductivity of the nanocomposite membrane is higher than the sample PVDF membrane. Our result matched with Arrhenius relationship which can be expressed by the following equation:

$$\sigma_{dc} = \sigma_0 exp_{kbT}^{-\Delta E} \quad (6)$$

where ΔE, *kb*, σ_o represent the thermal activation energy, Boltzmann's constant (8.617×10^{-5} eV/K), and pre-exponential factor/maximum conductivity, respectively [17].

Figure 11 illustrates the temperature dependence of conductivity, where the slopes of both composite samples are negative and almost linear.

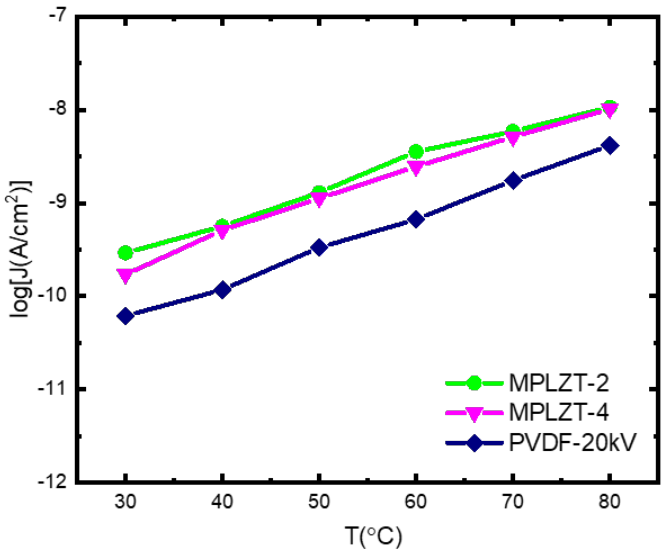

Figure 10. Current density versus temperature of MPLZT-2 and MPLZT-4 and PVDF-20kV at the applied voltage of 10V.

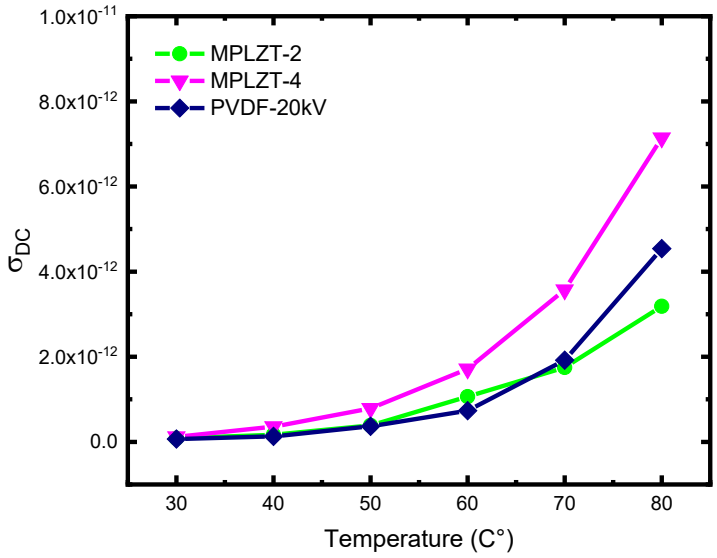

Figure 11 DC Conductivity with varying temperature for MPLZT-2 and MPLZT-4 and PVDF-20kV electrospun films at an applied voltage of 10V.

The calculated activation energy was found to be 0.79 eV, 0.77 eV, and 0.80 eV, respectively for samples MPLZT-2, MPLZT-4, and PVDF films as per Figure 12. The activation energies obtained via dc conductivity measurements are slightly different in the composite films [33] and the relatively small difference in the activation energies is indicative of the dynamically heterogeneous nature of PLZT aggregates within the polymer matrix [34].

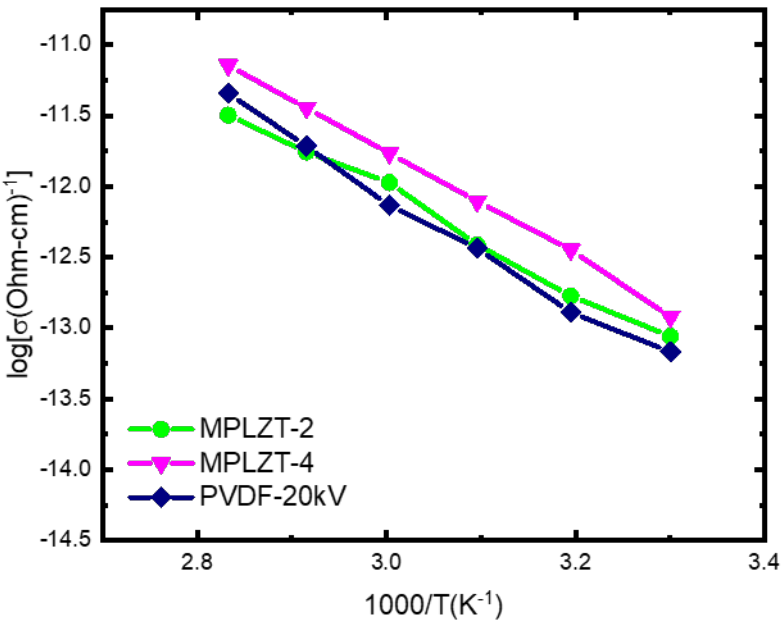

Figure 12. Temperature dependence of dc conductivity for MPLZT-2 and MPLZT-4 and PVDF-20kV at the applied voltage of 10V.

4. Conclusion and Future Recommendations

For the present investigation, PLZT nanocomposite films in a PVDF matrix were produced by the traditional electrospinning process. It is widely known that PVDF is a piezoelectric material and has applications from vibration sensing to energy harvesting. The addition of PLZT to the PVDF matrix enhances the dielectric response. To characterize such responses and to apply these characteristics to devices for tactile sensing, pressure transducers, energy harvesting, and vibration monitoring, it is critical to identify characteristics of these composites of PVDF and PLZT. Furthermore, the temperature dependency of electrical conductivity identifies the charge carrier transport mechanism to see if one or more mechanisms are involved in the conduction mechanism. It was determined that in comparison to pure PVDF, the PVDF-based nanocomposite films exhibit increased conductivity. It was also observed that the space charge limited current (SCLC) mechanism was dominant at high voltage, while the Schottky–Richardson conduction mechanism dominated at high temperature, according to our J–V characteristics. The dc activation energy was found to be slightly different for these composites and follow the Arrhenius relationship, which showed that the conduction was electronic and thermally activated. The electrical characteristics, therefore, provide more insight into the conduction mechanism in these functional polymer composites and are extremely useful in devices for appropriate applications. Since the fabrication parameters matrix is extremely large, the characterization can yield optimum results to optimize the fabrication process, almost similar to Taguchi's method. of parametric optimization.

FUNDING: This work was supported in part by the Title III program under Historically Black Graduate Institutions (HBGI) programs at Alabama Agricultural and Mechanical University, USA.

ACKNOWLEDGMENTS: The authors thank Dr. M.D. Aggarwal for his support and encouragement. Thanks go to Mr. E. Curtis for the fabrication of mechanical fixtures used in the present work. Authors duly acknowledge Mr. R. Paul for his technical assistance with scanning electron microscopy.

CONFLICT OF INTEREST: The authors declare no conflict of interest.

INSTITUTIONAL REVIEW BOARD: Human subjects were not involved in this study.

REFERENCES

1. P. Benaben, X. Boddaert, Design and development of printed acoustic sensor, Flexible Printed Electron. 1, 015001 (2016)
2. A. Alomari, A. Batra, M. Aggrawal, C.R. Bowen, A multi-source energy harvesting utilizing highly efficient ferroelectric PMN-PT single crystal J. Mater. Sci.(2016) doi:10.1007/s10854-016-5073-5
3. G. Sebald, L. Seveyat, D. Guyomar, L. Lebrun, B. Guiffard, S.Pruvost, Electrocaloric and pyroelectric properties of $0.75Pb(Mg_{1/3}Nb_{2/3})O_3–0.25PbTiO_30.75Pb(Mg_{1/3}Nb_{2/3})O_3–0.25PbTiO_3$ single crystals, J. Appl. Phys. 100, 124112 (2006)
4. R. Zhang, B. Jiang, W. Cao Elastic, piezoelectric, and dielectric properties of multidomain 0.67 Pb (Mg 1/3 Nb 2/3) O 3–0.33 PbTiO3 single crystals, J, Appl. Phys. 7, 90 (2001).
5. G. Kalimuldina, N. Turdakyn, I. Abay, A. Medeubayev, A. Nurpeissova, D. Adair, Z. Bakenov. A Review of Piezoelectric PVDF Film by Electrospinning and Its Applications. Sensors (Basel). 2020 Sep 12;20(18):5214. DOI: 10.3390/s20185214. PMID: 32932744; PMCID: PMC7570857.
6. P. Saxena, P. Shukla, A comprehensive review on fundamental properties and applications of poly(vinylidene fluoride) (PVDF). Adv Compos Hybrid Mater 4, 8–26 (2021). https://doi.org/10.1007/s42114-021-00217-0
7. M. Poulsen, S. Ducharma, Why Ferroelectric Polyvinylidene Fluoride is Special, IEEE Trans. Dielec. Electric. Insul.17, 1028 (2010)
8. K.J. Arun, A.K. Batra, A. Krishna, K. Bhat, M.D. Aggarwal, Surfactant Free Hydrothermal Synthesis of Copper Oxide Nanoparticles, Am. J. Mater. Sci. 5, 36 (2015)
9. M. Ohring, The Materials Science of Thin Films (Academic Press, San Diego, CA, 1992)
10. D.M. Taylor, T.J. Lewis, Electrical conduction in polyethylene terephthalate and polyethylene films, J. Phys. D 4, 1346 (1971).
11. D. R. Lamb, Electrical Conduction Mechanisms in Thin Insulating Films, Methuen, London, UK, 1967.
12. M. A. Lambert and P. Mark, Current Injection in Solids, Academic Press, New York, NY, USA, 1970.
13. J. G. Simmons, “Electronic conduction through thin insulating films,” in Handbook of Thin Film Technology, L.MaisselandR. Glang, Eds., chapter 14, McGraw-Hill, New York, NY, USA, 1970.
14. J. J. O’Dwyer, The Theory of Electrical Conduction and Break-down in Solid Dielectrics, Clarendon Press, Oxford, UK, 1973.

15. N.F.Mott and E.A. Davis, Electronic Processes in Non-Crystalline Materials, Oxford University Press, Oxford, UK, 1979.
16. A. Vaseashta, "Controlled formation of multiple Taylor cones in electrospinning process", Appl. Phys. Lett. 90, 093115 (2007) https://doi.org/10.1063/1.2709958.
17. N. Bölgen, A. Vaseashta, (2016) Nanofibers for Tissue Engineering and Regenerative Medicine. In: Sontea V., Tiginyanu I. (eds) 3rd International Conference on Nanotechnologies and Biomedical Engineering. IFMBE Proceedings, vol 55. Springer, Singapore. https://doi.org/10.1007/978-981-287-736-9_77.
18. A. Vaseashta, (2018) Loaded Electrospun Nanofibers: Chemical and Biological Defense. In: Bonča J., Kruchinin S. (eds) Nanostructured Materials for the Detection of CBRN. NATO Science for Peace and Security Series A: Chemistry and Biology. Springer, Dordrecht. https://doi.org/10.1007/978-94-024-1304-5_3.
19. S. Palwai, A. Batra, S. Kotru, and A. Vaseashta, Electrospun Polyvinylidene Fluoride Nanofiber Membranes Based Flexible Capacitive Sensors For Tactile and Biomedical Applications. Surface Engineering and Applied Electrochemistry, Vol. 58(1). 2022.
20. M. Chybiicki, Electrical properties of metal–polymer-metal (MPM) and metal-polymer–silicon (MPS) structures with thin polymer films, Phys. Status Solidi 39A, 271 (1977)
21. P.C. Mehendru, N.L. Pathak, S. Sing, P. Mehendru, Electrical conduction in polypropylene thin films, Phys. Status Solidi 38A, 255 (1976)
22. G. Caserta, B. Rispoli, A. Serra, Space-Charge-Limited Current and Band Structure in Amorphous Organic Films, Phys. Status Solidi 35B, 237 (1969)
23. P.G. Le Comber, J. Mort, eds. Electronic and Structural Properties of Amorphous Semiconductors (Academic Press, New York, 1973)
24. A. Batra, A. Alomari, M. Thomas, Dielectric Behavior of Paint/PZT Nanocomposite Films Br. J. Appl. Sci. Technol.7(2), 213–222 (2015)
25. D. K. Schroder, Semiconductor Material and Device Characterization, John Wiley & Sons, New York, NY, USA, 2nd edition, 1998.
26. F.H. Abd-El Kader, W.H. Osman, R.S. Hafez, DC conduction mechanism and dielectric properties of Poly (methyl methacrylate)/Poly (vinyl acetate) blends doped and undoped with malachite green, Physica B 408,140 (2013)
27. M.M. Kamal, A.H. Bhuiyan, Temperature Dependence of DC Electrical Conduction in Plasma Polymerized Pyrrole Thin Films, J. Mod. Sci. Technol. 2, 1 (2014)

28. A.A. El Tayyan, A. Khogali, DC Conduction in Fe3+ Poly(9-vinyl carbazole) Doped Films, Chin. J. Phys. 42, 392 (2004)
29. R. Martin, A.H. Bhuiyan, Electrical transport mechanism in plasma polymerized 2, 6, diethylaniline thin films, Thin Solid Films 519, 3462 (2011)
30. P. Saxena, M.S. Gaur, Electrical conduction mechanism of polyvinylidene fluoride (PVDF) – polysulfone (PSF) blend film, J. ELECTROSTAT. 67, 844 (2009)
31. M. Khissi, M. El Hasnaoui, J. Belattar, M.P.F. Graca, M.E. Achour, L.C. Costa, DC electrical conductivity studies on copolymer/carbon black composites, J. Mater. Environ. Sci. 2, 281 (2011).
32. J. G. Simmons, "Richardson-Schottky effect in solids," Physical Review Letters, vol. 15, no. 25, pp. 967–968, 1965.
33. P. Photopoulos, C. Tsonos, I. Stavrakas, D. Triantis, A method for the calculation of the activation energies of thermally stimulated depolarization current peaks: Application in polyvinylidene fluoride/graphene nanocomposites, Physica B: Condensed Matter (622), 2021, 413338, ISSN 0921-4526. https://doi.org/10.1016/j.physb.2021.413338.
34. B. B. Bohara, A. Batra, C.R. Bowen, Lanthanum-modified lead zirconate titanate based paint for sensor and energy harvesting applications. J Mater Sci: Mater Electron 29, 20931–20941 (2018). https://doi.org/10.1007/s10854-018-0237-0.